Pulsed laser deposition of Fe-oxypnictides: Co- and F-substitution

S. Haindl[1], M. Sato[2], S. Wurmehl[3], B. Büchner[3], E. Kampert[4]

[1] Tokyo Tech World Research Hub Initiative (WRHI), Institute of Innovative Research, Tokyo Institute of Technology - 4259 Nagatsuta-cho, Midori-ku, Yokohama, Kanagawa 226-8503, Japan
[2] Materials Research Center for Element Strategy, Tokyo Institute of Technology, 4259 Nagatsuta-cho, Midori-ku, Yokohama, Kanagawa 226-8503, Japan
[3] Institute for Solid State Research, IFW Dresden - Helmholtzstr. 20, 01069 Dresden, Germany
[4] Dresden High Magnetic Field Laboratory (HLD-EMFL), Helmholtz-Zentrum Dresden-Rossendorf - 01328 Dresden, Germany

E-mail: haindl.s.aa@m.titech.ac.jp

Abstract. The majority of thin film studies that were devoted to Fe-oxyarsenides has focused so far on F-substituted (i. e. indirectly electron doped) LnOFeAs (Ln = La, Nd, Sm). Here we turn our attention towards Co-substituted (i. e. directly electron doped) LaOFeAs and SmOFeAs in order to investigate its growth on different substrate materials by using pulsed laser deposition (PLD). We detected dominant LnOFeAs phase formation and discuss the occurrence of minor impurity phases in the different films on different substrates. The lack of a superconducting transition in $Ln\mathrm{OFe_{0.85}Co_{0.15}As}$ films on MgO(100) could be due to strain, since we observe an onset of superconductivity in $\mathrm{SmOFe_{1-x}Co_xAs}$ (x = 0.07, 0.15) films on other oxide substrates. In addition, Co-substitution (i.e. within the $\mathrm{Fe_2As_2}$ layers) and F-substitution (i.e. within the $Ln_2\mathrm{O_2}$ layers) leading to direct and indirect electron doping respectively, appears for films deposited on $\mathrm{CaF_2}$ substrates. In contrast to the F-substituted but Co-free Fe-oxyarsenides, the co-doped $\mathrm{SmO_{1-x}F_xFe_{0.85}Co_{0.15}As}$ film has experimentally accessible upper critical fields down to the lowest temperatures and may serve as an ideal test bed for further theoretical modeling of Fe-oxyarsenides.

PACS numbers: 74.70.Xa, 81.15.Fg, 74.25.-q

1. Introduction

Since the announcement of superconductivity in LnOFeAs (Ln = La, Nd, Sm) with ZrCuSiAs-type structure [1, 2, 3], their thin film synthesis was developed in several stages for different methods including *1)* post-annealing of deposited precursor films [4, 5, 6, 7, 8, 9, 10], *2)* molecular beam epitaxy (MBE) [11, 12, 13, 14, 15], and *3)* pulsed laser deposition (PLD) [16, 17, 18, 19, 20]. The incorporation of fluorine (F) as an electron dopant turned out to be the main challenge. Focusing on an *in-situ* PLD-growth process, the volatile nature of F impedes its stoichiometric transfer from the target to a heated substrate and even the conventionally chosen approach (i.e. enrichment of the target with the volatile element) is not applicable here [18, 21, 22]. Progress was made after finding a possible F-supply from alkaline earth fluoride substrates, $Ae\mathrm{F}_2$ (Ae = Ca, Sr, Ba) [17]. F-diffusion from various overlayers, buffer layers or CaF_2 substrates was also observed in the MBE-growth of $Ln\mathrm{O}_{1-x}\mathrm{F}_x$FeAs films [11, 12, 15]. In addition, F-diffusion from CaF_2 substrates finally enabled an *in-situ* PLD-growth of Fe-oxyarsenides. As a result, LnOFeAs films grown on CaF_2 substrates show a superconducting transition as well as less impurity phase formation. The chemical composition of these films is characterized by a F-diffusion gradient and the films can be described as layered hybrid structures with a F-rich layer near the substrate and a F-poor layer near the surface of the film [20].

The vast majority of the activities in film growth of LnOFeAs focused on F-substitution, primarily because of the superior critical superconducting parameters (T_c, H_{c2}, J_c). Here, we demonstrate and discuss PLD-growth of Co-substituted Fe-oxyarsenide films on different substrates. In comparison, the maximum transition temperatures for $\mathrm{LaO}_{1-x}\mathrm{F}_x$FeAs and $\mathrm{LaOFe}_{1-x}\mathrm{Co}_x$As are 26 K and 14.3 K, respectively (both for $x = 0.11$) [1, 23]. For $\mathrm{SmO}_{1-x}\mathrm{F}_x$FeAs and $\mathrm{SmOFe}_{1-x}\mathrm{Co}_x$As the maximum T_c is found at 55 K and 17.2 K, respectively (both for $x = 0.10$) [2, 24]. Whereas F- and Co-substitutions are commonly regarded as indirect and direct electron doping of the $\mathrm{Fe}_2\mathrm{As}_2$-layer, the subtle nuances between them have further spurred the discussion on the superconducting mechanism [25, 26]. In addition, the choice of Co-substitution has two advantages: First, from an engineering point of view, it offers an alternative to volatile dopants in studying the film growth of Fe-oxyarsenides. Exemplarily, $\mathrm{NdOFe}_{1-x}\mathrm{Co}_x$As films were first prepared by Corrales-Mendoza *et al.* [8] in developing a chemical vapor deposition (CVD) process for the growth of $\mathrm{NdO}_{1-x}\mathrm{F}_x$FeAs. Second, because of the lower critical parameters, the upper critical fields, $\mu_0 H_{c2}$, are experimentally much better accessible in Co-substituted than in the F-substituted LnOFeAs, which facilitates the comparison with theoretical models. The Co-substituted Fe-oxyarsenides can thus be regarded as a practical test bed for further investigations of the pairing mechanism, as was already pointed out by Charnukha *et al.* in an angle-resolved photoemission spectroscopy study on single crystals [27]. A recent investigation of $\mathrm{LaOFe}_{1-x}\mathrm{Co}_x$As claims the presence of a nematic quantum critical point around the optimal doping level [28]. Insofar, strain experiments in thin films may help to elucidate the role of nematic fluctuations in these compounds.

Here, we discuss film growth experiments using ultra-high vacuum (UHV) PLD where we have replaced F-substitution by Co-substitution with the aim to disentangle structural issues in film growth (lattice misfit, strain, etc.) from the usual difficulties of electron doping by F-substitution. Our analysis, therefore, addresses the transfer of $Ln\mathrm{OFe}_{1-x}\mathrm{Co}_x$As film growth to different oxide substrates, where we compare growth on MgO(100), LaAlO_3(100) and $\mathrm{MgAl}_2\mathrm{O}_4$(100). We have chosen different substrates, because the strain exerted by the substrate can influence the superconducting transition in the film. In comparison, co-doping of SmOFeAs with F- and Co-substitution is investigated on CaF_2 substrates. The upper critical field of a $\mathrm{SmO}_{1-x}\mathrm{F}_x\mathrm{Fe}_{0.85}\mathrm{Co}_{0.15}$As film was determined for temperatures down to 1.9 K.

2. Experimental

Thin film growth was carried out by PLD using a Spectra Physics Quanta Ray INDI Nd:YAG(2ω) laser (λ = 532 nm, repetition rate = 10 Hz, pulse width < 10 ns) in an UHV chamber with base pressure in the range of 10^{-9} – 10^{-8} mbar. The targets were ablated with a laser fluence of 2 – 3 Jcm^{-2} and the target-substrate distance was kept below 3 cm. We investigated film deposition on various single crystalline substrates MgO(100), LaAlO_3(100), $\mathrm{MgAl}_2\mathrm{O}_4$(100), and CaF_2(100) under similar conditions as given in refs. [17, 19]. For the film growth on LaAlO_3 and $\mathrm{MgAl}_2\mathrm{O}_4$ slightly higher substrate temperatures (∼900°C) were also

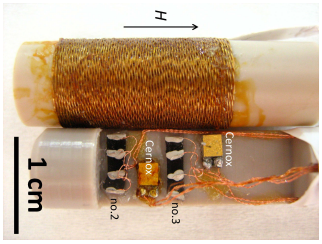

Figure 1. Two rectangular pieces (nos.2,3) cut from the original $SmO_{1-x}F_xFe_{0.85}Co_{0.15}As$ film sample (no.1) and mounted on the sample rod (H⊥c) for electrical transport measurements in pulsed magnetic fields. Two Cernox temperature sensors are mounted close to each film sample. The heater coil, that surrounds the samples, is shown above. The direction of the magnetic field is indicated by an arrow.

investigated. The oxide substrates were baked in air at 1000°C for 2 h before they were inserted into the UHV environment. $CaF_2(100)$ substrates were not subjected to any pretreatment.

Here we investigate Co-substituted Fe-oxyarsenides because Co is non-volatile and is expected to obey stoichiometric transfer from the target to the substrate. Co^{2+} substitutes for Fe^{2+}. All given Co-contents (x) are nominal values and we expect that the Co-content in the Fe-oxyarsenide phase is close to the nominal value. A quantification of the Co-content was undertaken by Auger electron spectroscopy (AES) based on relative sensitivity factors for two different thin film samples and confirmed the Co-contents of $x = 0.07$ and $x = 0.15$, respectively. AES depth profiling on the thin film samples also confirmed that Co is distributed uniformly across the film thickness. AES and depth profiling were carried out in an ULVAC-PHI 710-AES system using a primary electron beam energy of 10 kV and an electron current of 10 nA on a sample area of 150 μm in diameter. AES depth profiles were obtained by Ar^+ ion sputtering (1 kV, 2×2 mm^2). Spectra were recorded for kinetic energies of 40 – 150 eV, 455 – 860 eV and 1200 – 1410 eV with a step size of 1 eV (Details are given in Appendix C). For the film grown on CaF_2 substrate we expect a bilayer structure with a thin layer at the film/substrate interface having Co- and F-substitutions and a thicker layer on top with only Co-substitution analogous to the films in ref. [20].

Polycrystalline targets of $LaOFe_{1-x}Co_xAs$ ($x = 0.15$) and $SmOFe_{1-x}Co_xAs$ ($x = 0.07$ and 0.15) were prepared by a solid state reaction (see Refs. [29, 30, 31]), First, LaAs and SmAs, respectively, were prepared by sublimation of As in evacuated quartz tubes (10^{-6} mbar) using chunks of the corresponding lanthanide element (Ln) and As lumps in a 1:1 ratio. For the second step, the resulting LnAs was mixed with metallic Fe, Fe_2O_3 and metallic Co in the corresponding stoichiometric ratio. Each mixture of precursors was homogenized by grinding with a ball mill. For each target composition, the resulting homogeneous powder was pressed into several pellets under Ar atmosphere using a force of 20 kN and subsequently annealed in an evacuated quartz tube applying a temperature profile with two different dwell times at two different temperature regimes (940°C with 8 h dwell time, then heating up to 1150°C, dwelling at this temperature for 48 or 72 h). This synthesis route is similar to the one described in ref. [31].

The deposited films were characterized by X-ray diffraction (XRD) in a Rigaku Smart Lab (Cu Kα). The c-axis lattice parameters were evaluated from $2\theta/\omega$ scans performed in Bragg Brentano geometry with a typical step size of $\Delta 2\theta = 0.02°$. The total film thickness was evaluated by X-ray reflectivity (XRR) measurements that were performed in a parallel beam configuration using a Ge(220) crystal. Film thicknesses are in the range of 54 ± 12 nm. Atomic force microscopy (AFM) images were recorded in a Bruker AXS MultiMode8 atomic force microscope in non-contact mode using silicon tips on nitride cantilevers ($f \approx 130$ kHz, $k = 0.4$ Nm^{-1}). Typically, the scan size of the images was 1×1 μm^2 (512×512 pixel arrays). AFM images were processed with the software WSxM [32].

Superconductivity of the films was probed by temperature dependent electrical transport measurements in a Quantum Design Physical Property Measurement System (PPMS). For all electrical contacts Cu wires (0.1 mm in diameter) were attached with a conventional silver paste. The superconducting transitions are evaluated by resistance criteria (usually 90% R_n), for incomplete superconducting transitions the onset, $T_{c,on}$, was evaluated. For the determination of the upper critical field diagram, $\mu_0 H_{c2}(T)$, of the $SmO_{1-x}F_xFe_{0.85}Co_{0.15}As$ thin film, multiple electrical transport measurements were carried out in static and pulsed magnetic fields oriented parallel and perpendicular to the c-axis of the film: First, the temperature dependent resistance, $R(T)$, of the complete film sample (no.1) was measured in van der Pauw geometry in static magnetic fields up to 9 T with a current of 10 μA. After cutting the original thin film sample, $R(T)$ of a rectangular piece (no. 2) was measured in static magnetic fields up to 14 T with a current of 100 μA. Electrical transport measurements in pulsed magnetic fields ($\mu_0 H_{max} \approx 62$ T, pulse duration = 150 ms) were carried out on two rectangular film pieces (nos.2,3) at the Dresden High Magnetic Field Laboratory with AC currents of 100 μA and frequencies of 16 – 25 kHz (fig. 1). The thin film resistance was evaluated through a digital lock-in procedure on the measured sample voltages, recorded with a 1 MS/s 16-bit Yokogawa DL750 oscilloscope. The corresponding magnetoresistance data $R(\mu_0 H)$ for increasing magnetic fields is

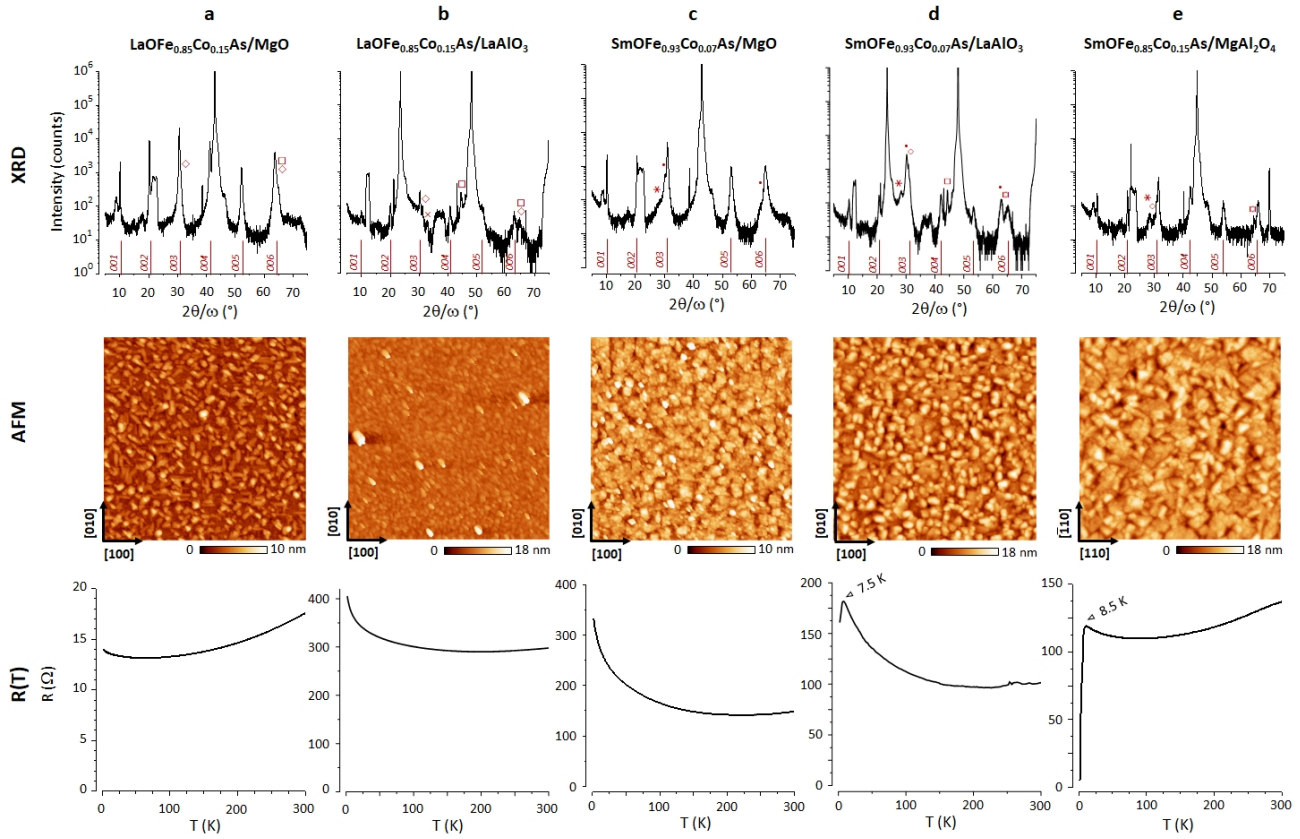

Figure 2. XRD intensities ($2\theta/\omega$ scans) with (00l) reflections of the Fe-oxyarsenide, impurity peaks of Fe (□), $FeAs_2$ (◇), SmAs (•) and Sm_2O_3 (∗) and misaligned grains (×) (top line), surface morphology of the film scanned by AFM (1×1 μm^2) with arrows indicating the orientation of the substrate (center line), electrical resistance as a function of temperature, $R(T)$, (bottom line) for a) $LaOFe_{0.85}Co_{0.15}As/MgO(100)$ ($c = 8.76$ Å); b) $LaOFe_{0.85}Co_{0.15}As/LaAlO_3(100)$ ($c = 8.88$ Å); c) $SmOFe_{0.93}Co_{0.07}As/MgO(100)$ ($c = 8.64$ Å) d) $SmOFe_{0.93}Co_{0.07}As/LaAlO_3(100)$ ($c = 8.58$ Å) and e) $SmOFe_{0.85}Co_{0.15}As/MgAl_2O_4(100)$ ($c = 8.52$ Å).

shown in figs. 4b,c. The temperature was controlled using a liquid ^{4}He bath cryostat and a local heater near the films, which were placed inside a stainless steel jacket with a He atmosphere. The temperature was monitored with two Cernox temperature sensors near the films. In particular, at temperatures below 4.2 K a hysteretic behavior of the magnetoresistance was found for magnetic fields ramped up and down, $R(\mu_0 H \downarrow) > R(\mu_0 H \uparrow)$, which could be attributed to a small, but noticeable temperature increase (∼0.5 K) during the complete magnetic pulse. These temperature variations are most likely caused by pressure instabilities in the liquid ^{4}He surrounding the samples, due to eddy currents in the stainless steel cryostat induced by the high magnetic flux change. The results shown below and the subsequent analysis were performed on the data obtained in increasing magnetic field, during which the temperature increase of the sample was minor.

3. Results and Discussion

3.1. Fe-oxypnictide thin film growth on oxide substrates

Crystalline Co-substituted *Ln*OFeAs thin films were grown on oxide substrates such as MgO(100), $LaAlO_3(100)$ and $MgAl_2O_4(100)$. Selected results are shown in fig. 2. For a pseudomorphic film growth, the lattice misfit $f = (a_f - a_s)/a_f$ between film (a_f) and substrate (a_s) at the growth temperature is a decisive parameter. At present, no information about the thermal lattice expansion of *Ln*OFeAs is available for the high temperature region (600 – 900°C) at which Fe-pnictide film growth typically takes place. Linear thermal expansion coefficients, α, of Fe-oxyarsenides were measured only for relatively low temperatures where values of $\sim1.2\times10^{-5}$ K^{-1} at 250 K [33] or $\sim1.4\times10^{-5}$ K^{-1} at 300 K [34] were determined. Considering in a first approximation the film/substrate lattice misfit at room temperature, then MgO(100) has the largest, whereas the spinel compound $MgAl_2O_4(100)$ with its cubic lattice ($a = 8.08$ Å) has the smallest misfit.

In particular, for LaOFeAs the misfit with $MgAl_2O_4$ is less than 1% (Appendix A, table A1).

It is important to note that despite the large lattice mismatch between MgO(100) and LnOFe$_{1-x}$Co$_x$As at room temperature, epitaxial thin film growth can be achieved on MgO(100) [16, 19]. Domain epitaxy and/or an incoherent film/substrate interface can be expected. The Co-substituted films grown on MgO(100) also show strong (00l) reflections from the Fe-oxyarsenide phase. Although electron doping by Co-substitution should be present, no superconducting transition was found in the films on MgO (figs. 2a,c). These results may indicate a strained lattice, less well interconnected grains or anti-phase domain boundaries like previously reported in ref. [20], leading to an unfavorable microstructure for superconductivity in the thin films. A nominal Co-content of $x = 0.15$ in the films is also near the overdoped limit of superconductivity according to refs. [23, 24], which could explain the lack of superconductivity in the LaOFe$_{0.85}$Co$_{0.15}$As films. The interesting result, however, is found in the comparison of SmOFe$_{1-x}$Co$_x$As films on different oxide substrates, where films on $LaAlO_3$ and $MgAl_2O_4$ do show a superconducting transition. This result supports the idea that strain exerted by MgO substrates tend to suppress superconductivity in the films.

Regarding $LaAlO_3$(100) substrates, film growth and the optimization of the deposition parameters for the *in-situ* PLD process were yet less controllable, although $LaAlO_3$ was previously successfully employed in the growth of LaO$_{1-x}$F$_x$FeAs films using a two-stage process [4]. In the latter, epitaxial films could be achieved through the formation of a LaOF interfacial layer during *ex-situ* post annealing [6, 21]. A SmOF impurity phase also appeared in SmO$_{1-x}$F$_x$FeAs films grown on $LaAlO_3$ by using MBE [15]. In PLD of LnOFe$_{1-x}$Co$_x$As, the high substrate temperatures favor the (001)-orientation but also the appearance of small amounts of Fe and $FeAs_2$ impurities (fig. 2b) or sustain Sm_2O_3, SmAs, $FeAs_2$ and Fe impurity phases in SmOFe$_{1-x}$Co$_x$As films (fig. 2d). In films deposited on $MgAl_2O_4$(100) substrates, the SmAs impurity was suppressed (fig. 2e). A list of identified impurity peaks in the here discussed Fe-oxyarsenide films is given in Appendix B (table B1). In all our films the c-axis lattice parameter is 0.5 – 2.2% larger compared to the bulk value. There is a diversity in surface morphologies mapped by AFM. Apart from droplets (common in PLD) the surfaces contain small grains of the Fe-oxyarsenide phase (best seen in fig. 2c) and differently shaped grains. The root-mean-squared (rms) surface roughness, R_q, of the films is between 1.1 and 2.8 nm. For SmOFe$_{1-x}$Co$_x$As incomplete superconducting transitions were found at $T_{c,on}$ = 7.5 K (SmOFe$_{0.93}$Co$_{0.07}$As/$LaAlO_3$) and $T_{c,on} = 8.5$ K (SmOFe$_{0.85}$Co$_{0.15}$As/$MgAl_2O_4$) (fig. 2d,e).

3.2. Oxypnictide thin film growth on CaF_2(100) and upper critical field

The deposition from a SmOFe$_{0.85}$Co$_{0.15}$As target on CaF_2(100) substrates resulted in Co- and F-substituted films. As reported in an earlier study [17], Fe-oxyarsenides grow with an epitaxial relation of [100](001)SmO(Fe,Co)As‖[110](001)CaF_2 and the lattice misfit between SmOFe$_{0.85}$Co$_{0.15}$As and CaF_2 is only ∼2.1%. The $2\theta/\omega$ scan shows sharp (00l) reflections and also a crystalline, metallic Fe impurity phase. Other impurities could not be detected, although a vanishingly small SmAs(002) impurity peak could be overlapped by the broad SmO$_{1-x}$F$_x$Fe$_{0.85}$Co$_{0.15}$As(003) (Appendix B). A regular pattern of small grains of quadratic shape can be seen on the surface. The film has a superconducting transition between 11.6 and 8.2 K (fig. 3). This value is close to the T_c of the target material and indicates that F-diffusion from the CaF_2 substrate did not raise the overall T_c. As shown in ref. [20] a F-gradient divides the films on CaF_2 into a F-rich layer close to the substrate and a F-poor layer towards the film surface. The approx. 10 nm thin film layer with F- and Co- co-doping is, therefore, close to the film/substrate interface and can be expected to shunt the superconducting current flow.

The simultaneous F- and Co-substitution ('co-doping') was first studied on polycrystalline bulk samples and demonstrated that additional Co-substitution deteriorates T_c in SmO$_{1-x}$F$_x$FeAs [35]. An investigation of the upper critical fields is yet missing. In our study here, the upper critical fields were first determined in static magnetic fields up to 9 T in van der Pauw geometry for the full thin film sample (no.1) (fig. 4a). For electrical transport measurements in linear geometry in pulsed magnetic fields, two rectangular pieces (nos.2,3) were cut from the original film sample (no. 1) (fig. 4b,c). In order to match the data points (i.e. the evaluation criteria) in the $\mu_0 H_{c2}(T)$-diagram for the complete sample (no.1) with those for its pieces (nos. 2 and 3), an additional measurement was made in static magnetic fields up to 14 T for sample no.2. Below 100 K the normal state resistance increases with decreasing temperature resulting in a crossover in the $R(\mu_0 H)$-curves (fig. 4c). The magnetoresistance becomes slightly negative with -0.12 ΩT^{-1}.

The upper critical fields (fig. 4d) can be modeled by a linear function for $H \parallel c$: $\mu_0 H_{c2,c}(T)$=20.88 − 1.8T, and by a quadratic function for $H \perp c$: $\mu_0 H_{c2,ab}(T) = 35.4 \cdot (1 - (T/11.6)^2)$. The Ginzburg-Landau coherence lengths evaluated from these fits are $\xi_{ab}(0) = 3.97$ nm and $\xi_c(0) = 2.34$ nm, respectively. These values represent upper limits of the coherence lengths in this film. The slopes of the upper critical fields

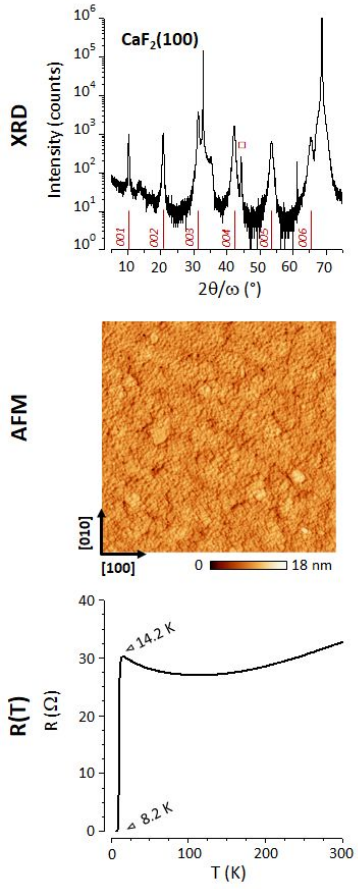

Figure 3. XRD intensities ($2\theta/\omega$ scan) of $SmO_{1-x}F_xFe_{0.85}Co_{0.15}As/CaF_2$. (00l) reflections are indicated and give a c-axis lattice parameter of 8.56 Å. Surface morphology scanned by AFM (1×1 μm^2). Arrows indicate the orientation of the substrate lattice. The rms roughness, R_q, is 1.7 nm. Temperature-dependent electrical resistance, $R(T)$, with a superconducting transition.

are accordingly $\mu_0(dH_{c2,c}/dT)_{Tc}$=−1.8 TK^{-1} and $\mu_0(dH_{c2,ab}/dT)_{Tc} = -6.1$ TK^{-1}. The corresponding Werthamer-Helfand-Hohenberg (WHH) [36] curves would underestimate (overestimate) $\mu_0 H_{c2,c}$ ($\mu_0 H_{c2,ab}$).

In reduced variables, $t = T/T_c$ and $h = H_{c2}/(T_c \cdot |dH_{c2}/dT|_{Tc})$, the temperature dependence as well as deviation from the WHH curve can be found: For $H \parallel c$ the reduced upper critical fields follow $h \propto 1 - t$ in the interval $t \in [0.3, 1]$. At the lowest accessible temperature of our measurement (1.9 K) the upper critical field is enhanced. A similar temperature dependence of $\mu_0 H_{c2}$ has already been observed in $LaO_{1-x}F_xFeAs$ [37] thin films (fig. 4e) and also in optimally doped $SmOFe_{0.92}Co_{0.08}As$ single crystals [38] where the reduced field parallel to the c-axis has a linear temperature dependence in the interval $t \in [0.5, 1]$, although $\mu_0 H_{c2}$ is larger than for our co-doped films due to a larger T_c (smaller Co-content). We finally note that a fit of the steep upturn of $\mu_0 H_{c2}$ at low temperatures in a two-band analysis could only be obtained with a high ratio of band diffusivities. A similar analysis was performed for $LaO_{1-x}F_xFeAs$ in ref. [6]. Additional knowledge about the electronic properties are, therefore, essential.

4. Conclusions

Co-substituted Fe-oxyarsenide thin films were fabricated by PLD on different oxide substrates and on CaF_2. Starting from optimal deposition parameters found for epitaxial film growth on MgO and CaF_2 substrates, predominant c-axis oriented and textured growth of LnOFe$_{1-x}$Co$_x$As was also found on $LaAlO_3$ and $MgAl_2O_4$ substrates. LnOFe$_{1-x}$Co$_x$As grows as main phase with c-axis-oriented texture, but the high substrate temperatures also favor Fe, $FeAs_2$, SmAs and Sm_2O_3 impurity growth. Fe impurities are always present, as it is common in PLD growth of Fe-pnictides. Whereas no superconducting transition was found for LnOFe$_{1-x}$Co$_x$As thin films deposited on MgO(100), the onset of a superconducting transition appears in $SmOFe_{1-x}Co_xAs$ films deposited on $LaAlO_3$(100) and $MgAl_2O_4$(100). We attribute the suppressed superconductivity on MgO mainly to strain. In comparison to oxide substrates, film deposition on CaF_2 substrates resulted in co-doped $SmO_{1-x}F_xFe_{0.85}Co_{0.15}As$ films of good crystalline quality and with a complete superconducting transition. The upper critical field of a $SmO_{1-x}F_xFe_{0.85}Co_{0.15}As$ film was investigated in detail and its temperature-dependence displayed an enhancement at lowest reduced temperatures qualitatively similar to $LaO_{1-x}F_xFeAs$ films fabricated by a two-stage process.

Acknowledgments

Funding: S. H. acknowledges the support from WRHI and funding from German Research Foundation (HA 5934/5-1). The work at IFW Dresden has been supported by the Deutsche Forschungsgemeinschaft (DFG) through the Priority Programs SPP1458 (BU887/15-1), DFG-GRK1621, and the Emmy-Noether project (WU595/3-3). *Author contributions:* S. H. was responsible for the design of the study, thin film growth, film characterization and the preparation of the manuscript. M. S. was responsible for AES measurements. E. K. was responsible for electrical transport measurements in pulsed magnetic fields. S. W. was responsible for target preparation and characterization. All authors discussed the results. All authors also acknowledge the support of the HLD-HZDR, a member of the European Magnetic Field Laboratory (EMFL). The authors thank H. Hiramatsu,

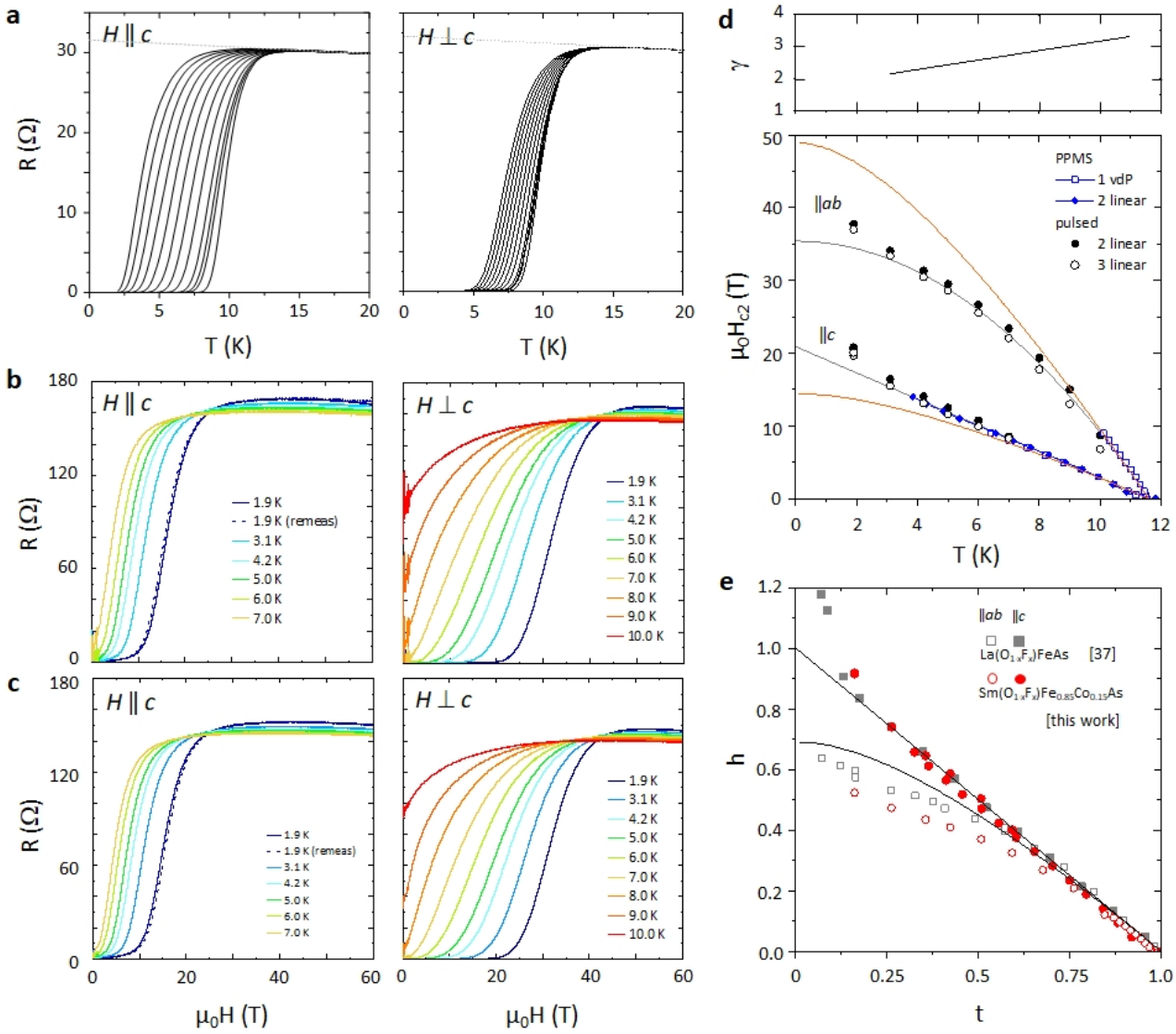

Figure 4. a) $R(T)$ of a $SmO_{1-x}F_xFe_{0.85}Co_{0.15}As$ film (1×1 cm^2) measured in van der Pauw geometry (no.1) in magnetic fields of 0, 0.25, 0.5, and 1 – 9 T in steps of 1 T (from right to left); b) and c) Magnetoresistance, $R(\mu_0 H)$, of two rectangular pieces of the $SmO_{1-x}F_xFe_{0.85}Co_{0.15}As$ film (compare fig. 1) measured in linear geometry (nos. 2,3). A re-measurement of the magnetoresistance at 1.9 K is also shown for $H \parallel c$ and demonstrates the reproducibility of the data point. d) Upper critical fields for a $SmO_{1-x}F_xFe_{0.85}Co_{0.15}As$ film grown on CaF_2 (samples nos.1–3). The evaluation criterion was 90% R_n (no.1) and 82% R_n (nos.2,3). The gray lines represent the linear and quadratic fits, from which the anisotropy of the upper critical fields, $\gamma = H_{c2,ab}(T)/H_{c2,c}(T)$ was evaluated. The red lines represent the WHH result for both directions. e) Comparison of the upper critical fields in reduced variables $h(t)$ of the PLD grown $SmO_{1-x}F_xFe_{0.85}Co_{0.15}As$ thin film (this work) and a $LaO_{1-x}F_xFeAs$ film fabricated by a two-stage process [22, 37, 39].

H. Hosono (both Tokyo Institute of Technology), and C. Malbrich, K. Leger, T. Möller, I. Dintzsch, S. Müller-Litvanyi and J. Werner (all IFW Dresden) for support and the late G. Behr (IFW Dresden) for fruitful scientific discussion.

Appendix A. Lattice misfits of hetero-oxide interfaces

We have calculated lattice misfits, f_{Ln1111}, between $LaOFe_{0.85}Co_{0.15}As$ (with $a_f = 4.035$ Å) respectively $SmOFe_{0.85}Co_{0.15}As$ (with $a_f = 3.938$ Å) film and substrate (at room temperature) [24]. The positive (negative) sign of f indicates that the film is compressed (stretched).

Table A1. Calculated lattice misfits (%) at room temperature.

substrate	a_S (Å)	$a_S/2$ (Å)	f_{La1111}	f_{Sm1111}
$LaAlO_3(100)$	3.79		+6.0%	3.8%
$MgAl_2O_4$	8.085	4.0425	-0.2%	-2.7%
MgO(100)	4.21		-4.3%	-6.9%

Appendix B. XRD and impurity phases

We note that all XRD reflections have been indexed. In general, the high tendency for impurity phase formation in PLD of Fe-oxyarsenide films reduces the reproducibility and makes optimization of the deposition parameters difficult. Crystalline impurity phases are usually detected in XRD but some reflections may be hidden by substrate peaks or overlapped by strong (00l) reflections of the Fe-oxyarsenide phase. The $FeAs_2$ impurity has its (001) and (002) reflections near $2\theta \approx 31.00°$ and $2\theta \approx 64.62°$. Since it appears both in $SmOFe_{1-x}Co_xAs$ as well as in $LaOFe_{1-x}Co_xAs$ films, a reflection of inclined domains with $SmOFe_{1-x}Co_xAs$(102) and (204) peaks near $2\theta \approx 31.02°$ and $2\theta \approx 64.68°$ may be ruled out. The Fe(002) peak is also located near $2\theta \approx 64.67°$. The indexed impurity peaks are listed in table B1. We also note that in contrast to Sm_2O_3 and SmAs impurities in $SmOFe_{1-x}Co_xAs$ films, neither La_2O_3 nor LaAs was present in $LaOFe_{1-x}Co_xAs$ films.

Table B1. Appearance (✓) of impurity phases in $LnOFe_{1-x}Co_xAs$ films as discussed in the text. Reflections for which no conclusive statement can be made because they may be hidden due to the overlap with other reflections (e.g. substrate or strong (00l) reflections of the $Ln1111$ phase) are denoted by (○). Absent reflections are denoted by (-).

film	Co-content	Fe(110)	Fe(002)	$FeAs_2$(001)	LaAs(002)	La_2O_3(222)	SmAs(002)	Sm_2O_3(222)
La1111/MgO	0.15	○	○	✓	○	-		
La1111/$LaAlO_3$	0.15	✓	✓	✓	○	○		
Sm1111/MgO	0.07	○	○	○			✓	-
Sm1111/$LaAlO_3$	0.07	✓	✓	✓			✓	✓
Sm1111/$MgAl_2O_4$	0.15	○	✓	✓			-	✓
Sm1111/CaF_2	0.15	✓	○	○			✓	-

Fig. B1 shows details of the $2\theta/\omega$ scans of the discussed $LnOFe_{1-x}Co_xAs$ and $SmO_{1-x}F_xFe_{0.85}Co_{0.15}As$ thin films in the range of $2\theta = 27 - 35°$.

Appendix C. AES concentrations

For $SmOFe_{0.85}Co_{0.15}As$ on $MgAl_2O_4$ and $SmOFe_{0.93}Co_{0.07}As$ on $LaAlO_3$ AES depth profiles were analyzed. From the Auger spectra the peak-to-peak intensities of Sm $N_{4,5}VV$, O $KL_{2,3}L_{2,3}$, Fe $L_3M_{4,5}M_{4,5}$,

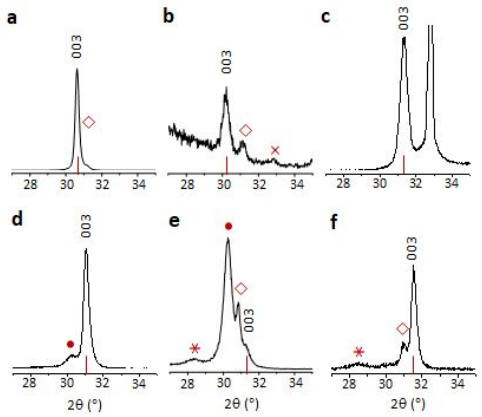

Figure B1. $2\theta/\omega$ scans around the $LnOFe_{1-x}Co_xAs(003)$ reflection (|) with $FeAs_2(001)$ (◇), SmAs(002) (●), $Sm_2O_3(222)$ (∗), and $LaOFe_{1-x}Co_xAs$ (111) (×) reflections: a) La1111/MgO(100) ($x_{Co} = 0.15$); b) La1111/$LaAlO_3$(100) ($x_{Co} = 0.15$); c) Sm1111/CaF_2(100) ($x_{Co} = 0.15$); d) Sm1111/MgO(100) ($x_{Co} = 0.07$); e) Sm1111/$LaAlO_3$(100) ($x_{Co} = 0.07$); f) Sm1111/$MgAl_2O_4$(100) ($x_{Co} = 0.15$).

Co $L_3M_{4,5}M_{4,5}$ and As $L_3M_{4,5}M_{4,5}$ were evaluated. Relative sensitivity factors were obtained in fixing the Sm-, O- and As-contents to 25 at.%, respectively. Quantification results based on relative sensitivity factors matched with the nominal Co-contents of $x = 0.15$ and $x = 0.07$ (fig. C1). Changes in the chemical composition only occur in a surface layer and near the film/substrate interface. No significant diffusion from the substrates into the films could be detected.

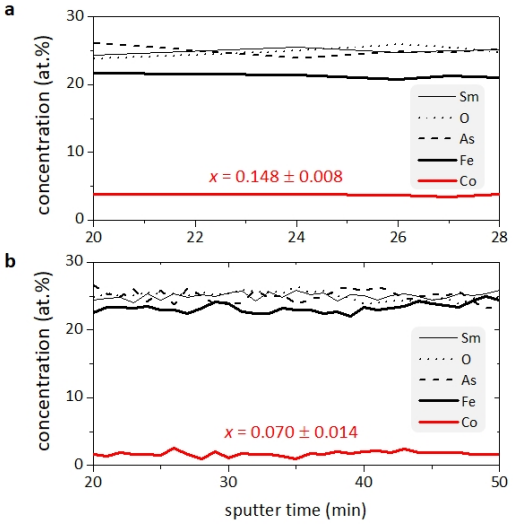

Figure C1. Concentrations (at.%) of Sm, O, Fe, Co and As in a) Sm1111/$MgAl_2O_4$(100) ($x_{Co} = 0.15$) and b) Sm1111/$LaAlO_3$(100) ($x_{Co} = 0.07$) measured in central parts of the films.

References

[1] Kamihara Y., Watanabe T., Hirano M., Hosono H., J. Am. Chem. Soc. 130, 3296 (2008)
[2] Ren Z.-A., Lu W., Yang J. *et al.*, Chin. Phys. Lett. 25, 2215 (2008)
[3] Pöttgen R., Johrendt D., Z. Naturforsch. 63b, 1135 (2008)
[4] Backen E., Haindl S., Niemeier T. *et al.*, Supercond. Sci. Technol. 21, 122001 (2008)
[5] Kidszun M., Haindl S., Reich E. *et al.*, Supercond. Sci. Technol. 23, 022002 (2010)
[6] Haindl S., Kidszun M., Onken F., Mietke A., Int. J. Mod. Phys. B 27, 1330001 (2013)
[7] Corrales-Mendoza I., Conde-Gallardo A. IEEE Trans. Appl. Supercond. 24, 7300106 (2014)
[8] Corrales-Mendoza I., Bartolo-Pérez P., Sánchez-Reséndiz V. M. *et al.*, Eur. Phys. Lett. 109, 17007 (2015)
[9] Corrales-Mendoza I., Llabias-Romero J., Castillo N., Conde-Gallardo A., Supercond. Sci. Technol. 32, 055005 (2019)
[10] Matsumoto J., Hanzawa K., Sasase M., *et al.*, Phys. Rev. Materials 3, 103401 (2019)
[11] Kawaguchi T., Uemura H., Ohno T., *et al.*, Appl. Phys. Lett. 99, 232505 (2011)
[12] Takeda S., Ueda S., Takano S., *et al.*, Supercond. Sci. Technol. 25, 035007 (2012)
[13] Sugawara H., Tsuneki T., Watanabe D., *et al.*, Supercond. Sci. Technol. 28, 015005 (2015)
[14] Chihara M., Sumiya N., Arai K., *et al.*, Physica C 518, 69 (2015)
[15] Ueda S., Takeda S., Takano S., Naito M., Appl. Phys. Express 5, 053101 (2012)
[16] Hiramatsu H., Katase T., Kamiya T., *et al.*, Appl. Phys. Lett. 93, 162504 (2008)
[17] Haindl S., Hanzawa K., Sato H., *et al.*, Sci. Rep. 6, 35797 (2016)
[18] Haindl S., Molatta S., Hiramatsu H., Hosono H., J. Phys. D: Appl. Phys. 49, 345301 (2016)
[19] Haindl S., Kinjo H., Hanzawa K. *et al.*, Appl. Surf. Sci. 437, 418 (2018)
[20] Haindl S., Kampert E., Sasase M. *et al.*, Supercond. Sci. Technol. 32, 044003 (2019)
[21] Haindl S., Kidszun M., Oswald S. *et al.*, Rep. Prog. Phys. 77, 046502 (2014)
[22] Haindl S., Kidszun M., Kampert E., Phys. Stat. Sol. B 254, 1600341 (2017)
[23] Sefat A. S., Huq A., McGuire M. A. *et al.*, Phys. Rev. B 78, 104505 (2008)
[24] Wang C., Li Y. K., Zhu Z. W. *et al.*, Phys. Rev. B 79, 054521 (2009)
[25] Wadati H., Efimov I., Sawatzky G. A., Phys. Rev. Lett. 105, 157004 (2010)
[26] Berlijn T., Lin C.-H., Garber W., Ku W., Phys. Rev. Lett. 108, 207003 (2012)
[27] Charnukha A., Thirupathaiah S., Zabolotnyy V. B. *et al.*, Sci. Rep. 5, 10392 (2015)
[28] Hong X., Caglieris F., Kappenberger R. *et al.*, *arXiv:1908.00484v1*
[29] Zhu X., Yang H., Fang L. *et al.*, Supercond. Sci. Technol. 21, 105001 (2015)
[30] Kondrat A., Hamann-Borrero J. E., Leps N. *et al.*, Europ. Phys. J. B 70, 461 (2009)
[31] Grafe H.-J., Lepucki P., Witschel M. *et al.*, Phys. Rev. B 101, 054519 (2020)
[32] Horcas I., Fernández P., Gómez-Rodriguez M. *et al.*, Rev. Sci. Instrum. 78, 013705 (2007)
[33] Klingeler R., Wang L., Köhler U. *et al.*, J. Phys.: Conf. Ser. 200, 012088 (2010)
[34] Wang L., Köhler, U., Leps N. *et al.*, Phys. Rev. B 200, 012088 (2009)
[35] Yang Z., Zhu L., J. Supercond. Nov. Magn. 27, 2035 (2014)
[36] Helfand E., Werthamer N. R., Phys. Rev. 147, 288 (1966)
[37] Kidszun M., Haindl S., Thersleff T., *et al.*, Phys. Rev. Lett. 106, 137001 (2011)
[38] Zhigadlo N. D., Weyeneth S., Katrych S., *et al.*, Phys. Rev. B 106, 214509 (2012)
[39] Kidszun M., PhD thesis (TU Dresden)